Probing the Ultrastructure of Spheroids and Their Uptake of Magnetic Nanoparticles by FIB–SEM

Probing the ultrastructure of spheroids and their uptake of magnetic nanoparticles by FIB-SEM

Valentina Mollo[1±], Paola Scognamiglio[1±], Attilio Marino[2], Gianni Ciofani[2,3], Francesca Santoro[1*]

[1]Center for Advanced Biomaterials for Healthcare, Istituto Italiano di Tecnologia, Naples, Italy.
[2]Smart Bio-Interfaces, Istituto Italiano di Tecnologia, Pontedera, Italy.
[3]Department of Mechanical and Aerospace Engineering, Politecnico di Torino, Torino, Italy.

[*]Correspondence to: francesca.santoro@iit.it

[±]these authors have equal contribution.

MANUSCRIPT

Abstract

Spheroids are 3D cellular systems largely adopted as model for high-throughput screening of molecules and diagnostics tools. Furthermore, those cellular platforms also represent a model for testing new delivery carries for selective targeting. The coupling between the 3D cell environment and the nanovectors can be explored at the macroscale by optical microscopy. However, the nanomaterial-cell interplay finds major action at the single cell and extracellular matrix level with nanoscale interactions. Electron microscopy offers the resolution to investigate those interactions, however the specimen preparation finds major drawbacks in its operation time and preciseness. In this context, focused ion beam and scanning electron microscopy (FIB-SEM) allows for fast processing and high resolution of the cell-nanomaterial interface. Here, in fact, we show a novel approach to prepare large-area 3D spheroid cell culture specimens for FIB-SEM. We explored sectioning procedures to preserve the peculiar structure of spheroids and their interaction with magnetic nanovectors. Our results pave the way for advanced investigations of 3D cellular systems with nano and micromaterials relevant to tissue engineering, bioelectronics and diagnostics.

Keywords: scanning electron microscopy, focused ion beam, spheroids, biointerfaces, nanocarriers, endocytosis.

Introduction

In the last decade, spheroid-like cellular architectures have become powerful model systems to biomimic complex tissue-like forms towards the fully recapitulation of organoid-like systems. In fact, these closed-systems are excellent tools for understanding complex cellular functions, testing new molecules for drugs and diagnostics solutions[1]. In this context, 3D tumor spheroids have been adopted as reliable model of *in vivo* solid tumors for the screening of different anticancer drugs and nanoformulations[2,3]. In comparison to 2D cancer cell cultures, tumor spheroids display many different features of the *in vivo* solid tumors (*e.g.*, spatial architecture, high-level secretion of soluble mediators, gene expression profile and multidrug resistance mechanisms)[4].

Our former studies, for instance, adopted spheroid-like tumoral system to evaluate the efficacy of lipid nanovectors have been loaded with superparamagnetic iron oxide nanoparticles (SPIONs)[5]. SPIONs efficiently generate heat when exposed to alternated magnetic fields (AMF) and have been successfully exploited for hyperthermia treatment of glioblastoma in clinical trials[6].

Furthermore, our group has recently developed lipid nanovectors loaded with both SPIONs and the temozolomide (TMZ) drug for the combined hyperthermia and chemotherapy treatment of glioblastoma cells[7]. For all these aforementioned applications (i.e. hyperthermia, MRI imaging and chemotherapy treatment), the nanovector accumulation inside the 3D tumor models is of crucial importance.

In this scenario, these 3D closed- systems and their interaction with nanomaterials have been so far largely investigated by means of optical microscopy techniques[8,9]. However, there are certainly limitations in terms of characterization of the inner spheroid interactions, achieved resolution and labelling of multiple cellular components. Alternatively, 3D cell architectures can be further inspected at the nanoscale by electron microscopy techniques. In fact, the typical polymeric embedding ensures that the 3D morphology is preserved and the cross sectioning allows for the investigation of specific thin sections and eventually the reconstruction of a volume of interest[10].

Transmission electron microscopy can be performed following a mechanical thin-sectioning, allowing for slice thickness in the range of ~70 nm[11]. Given the large size of 3D spheroids, this procedure would yield to hundreds of sections which might be collected and analyzed individually. This is an extremely time consuming process and recently, scanning electron microscopy coupled with in-chamber mechanical serial sectioning tools have provided an alternative approach for fast processing and imaging [12].

Here, serial block-face imaging scanning electron microscopy (SBF-SEM) and focus ion beam scanning electron microscopy (FIB-SEM) found major applications for morphological analysis of stem cell spheroids, organoids, as well as organotypic cell cultures.

SBF-SEM uses the automated ultramicrotome located inside the SEM chamber and removes sections (≥20 nm thick) from the block face and provides scanning of relatively large volumes.

Alternatively, focused ion beam- scanning electron microscopy (FIB-SEM) tomography is the most promising approach for 3D imaging at the subcellular level and is considered as a revolution for ultrastructural volume reconstruction[13–15] avoiding the drawbacks of mechanical sectioning procedures and achieving sections' thickness < 20 nm. In fact, this technique has been already adopted for the investigation of 2D and 3D cultures on diverse biomaterials[16–19] and the characterization of complex tissue-like architectures.[20,21]

In this work, we further exploit the FIB-SEM procedure to investigate regions of interest in 3D spheroid cell cultures and their interaction with magnetic nanovectors, which can penetrate and reach the spheroid inner domain. The spheroids have been macroscopically observed employing two specimens preparation procedures which include hard drying and resin-embedding processes. Given the large size of the spheroids, those have been initially mechanically sectioned to reduce their effective volume and be subsequently polished by focused ion beam. Finally, we characterize the interface between cell and extracellular matrix with magnetic nanovectors exploring the different phases of the SPIONs uptake process.

Results

3D spheroids have been obtained from U87 MG cells and assemble in a 3D architecture following the hanging-drop procedure (see **Experimental Section**). The U87 MG-derived spheroids were loaded with lipid magnetic nanovectors (LMNVs) labeled with a lipophilic fluorescent probe, which marked the lipid part of the vectors (24-48 hours of incubation). Nanovectors approach the surface of individual cells (**Figure 1A,** the scanning electron micrograph of spheroid also shows the interaction of LMNVs with its surface as shown by the blue arrows) and they further penetrate both in the intracellular and inter-cellular domains. In fact, **Figure 1B-D** show how cells and nanovectors simultaneously populate the spheroids.

Thus, through fluorescence imaging, the rate of penetration and the quantification of LMNVs inside the spheroids were calculated. In fact, after 24 hours 0.8 % (s.d.: +- 0.7 %) of the total volume of the spheroids were populated by LMNVs and after 48 hours this volume reaches 8.1% (s.d.:+- 0.5 %)[5]. To further evaluate the nanovector-spheroid interface interaction, we prepared the specimens for SEM/FIB milling and imaging.

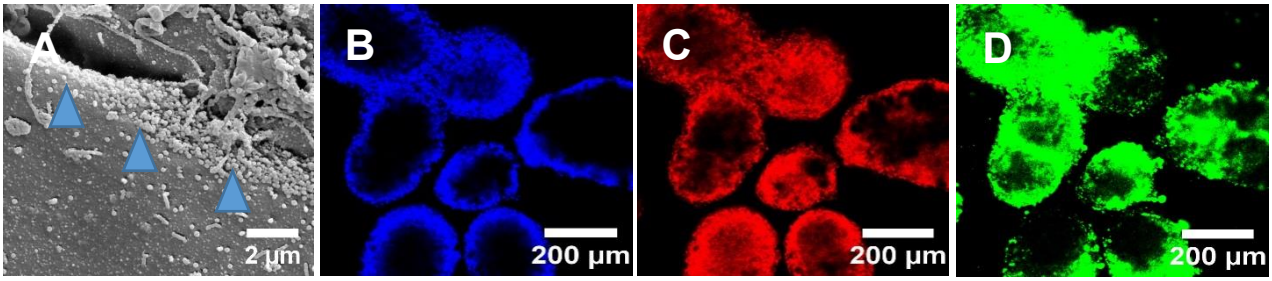

Figure 1: Morphology of U87_MG derived spheroids and nanovector internalization: A) Scanning electron micrograph of spheroid surface treated with ROTO protocol with lipid magnetic

nanovectors, LMNVs (blue arrow). B,C,D) confocal laser scanning microscopy imaging of spheroids: nuclei in blue (Hoechst) with fluorescent nanovectors in green and F-actin in red; scan area is 1273 µm x 1273 µm.

Due to the large size, sectioning *via* FIB of a whole spheroid (400-500 µm) would require extremely long processing times. For this reason, each spheroid was divided in to four parts during the fixation and embedding procedure. The cutting was carried out carefully with a small razor blade (see **Supplementary Information S1**). To assess the possible damages due to the mechanical sectioning (i.e. compression, breakages, eradication of organelles, etc.,), the ultrastructure of the spheroids was investigated after each step of cutting.

The ROTO-UTP (reduced osmium–thiocarbohydrazide–osmium ultra thin plasticization) protocol used for the specimen preparation is structured in nine main steps (**Figure 2**, Box A), in relation to the use of different substances for fixation and heavy-metal staining (glutaraldehyde, glycine, osmium tetroxide/potassium ferro-cyanide, thiocarbohydrazide, osmium tetroxide, uranyl acetate, tannic acid, ethanol, Spurr's resin). Among these procedure's steps, six were selected as a point in time when each spheroid was sliced in to four parts. Thus, we identify six cutting steps: step 1:after fixation in glutaraldehyde; step 2: after osmium tetroxide; step 3: after thiocarbohydrazide (TCH); step 4: after tannic acid; step 5: in resin embedding before polymerization; step 6: in resin after polymerization as described in **Figure 2** (**Box** A-B). After each cutting step, the each spheroid section was embedded according the ROTO-UTP protocol. Here, spheroids appear comparably soft during the cutting after fixation in glutaraldehyde. In fact, samples' hardness increased after the incubation with osmium tetroxide and thus the spheroids acquire resistance to cutting especially after the treatment with TCH (step 3).

It is known that the tannic acid used after glutaraldehyde and osmium tetroxide fixation improves the preservation of the cell features against shrinkage and thermal damage occurring during the sample preparation[22]. Here, when the tannic acid was added, the spheroids surface became fragile during the cutting (step 4) and at the outside part of the spheroid several cells collapsed (see **Supplementary Information S1**). After the embedding in Spurr's resin, spheroids became more resistant by comparing them to the other spheroids sliced in previous steps and intact during the sectioning procedure (step 5), especially after the final polymerization (step 6). The size of the whole spheroid was not s appreciably affected during the ROTO-UTP protocol as shown in **Figure**

2A (post glutaraldehyde fixation) and **Figure 2B** (in Spurr's resin embedding) and further discussed in see **Supplementary Information S1**).

Complementarily, the dehydration procedure through critical point drying (CPD) was carried out on whole spheroids as shown **in Figure 2 C,D**. During the CPD process, the most crucial step is in the final part of the procedure where the outflow of the gas of the supercritical carbon dioxide is carried out slowly in order to avoid the collapse of samples. (0.05 bar/sec).

Effectively, U87-based spheroids exhibited a complex 3D structure which expands over several hundreds of micrometers. Furthermore, the overall morphology have been investigated by secondary electrons detection after the drying procedures. Interestingly, spheroids prepared *via* CPD had individual cell bodies which appeared round and homogenously distributed throughout the whole spheroid area with no comparable collapsed regions. Here, at higher magnification, apical microvilli protrusions are clearly visible (**Figure 2 C-D**), however, when FIB cross sectioning was performed (**Supplementary Information S2**) no intact cellular ultrastructures were distinguishable because of the cavities and artefacts induced by the hard drying procedure[23].

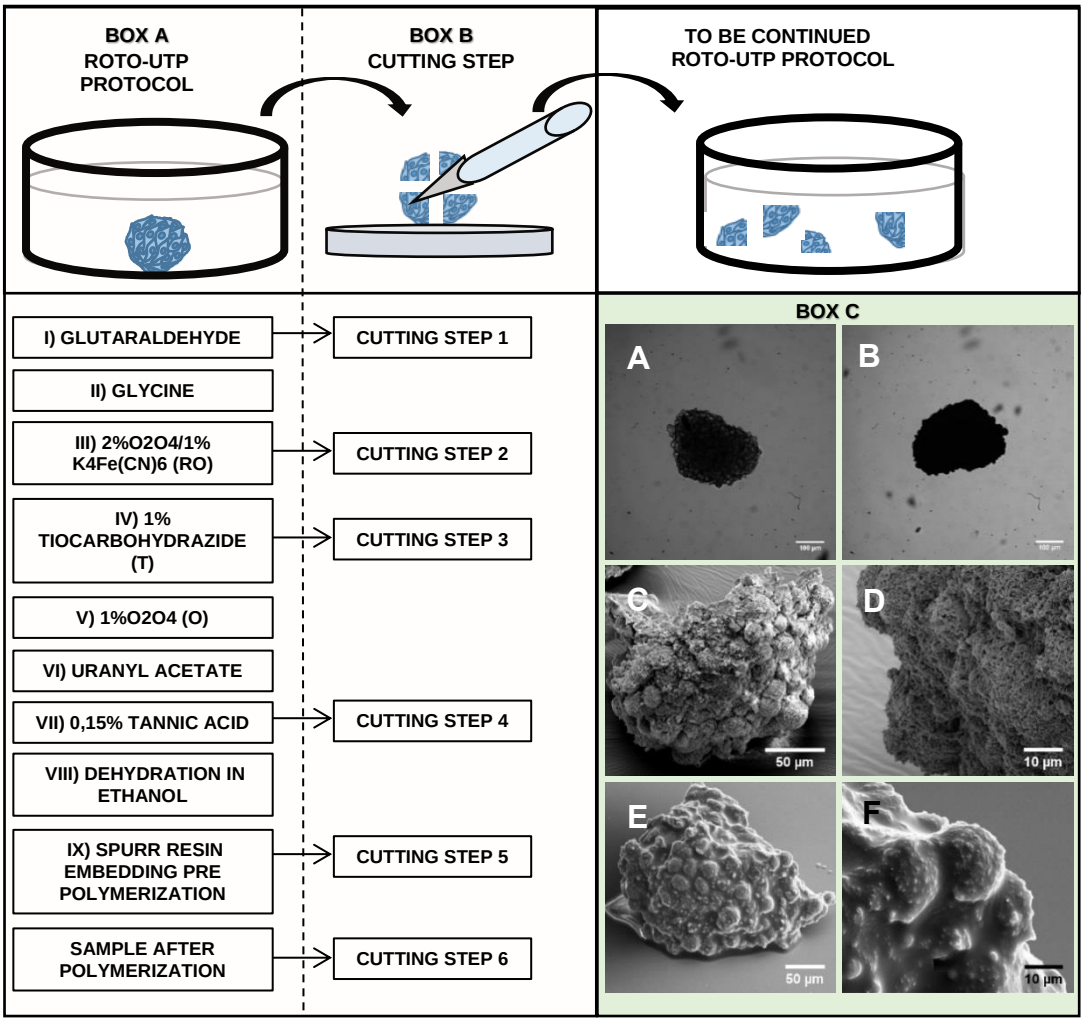

Figure 2: **SCHEMATIC FLOW OF SPECIMEN PREPARATION**. Box A summarizes the main points of the ROTO-UTP protocol (from I to IX) while in Box B the steps for the mechanical sectioning of the spheroids are reported. To evaluate the U87-MG derived spheroids ultrastructure a total of 18 spheroids were prepared with this procedure and, 3 spheroids were cut in four parts by using a razor blade at each set time points. After cutting, each sliced spheroid underwent ROTO-UTP procedure. Box C shows the size of an exemplary spheroid after fixation in glutaraldehyde (A) and its final morphology in Spurr's resin by using the optical microscope (B) and scanning electron microscope (E,F). C and D are scanning electron micrographs of whole U87-MG derived spheroids acquired in secondary electrons mode after critical point drying.

In parallel, following the ROTO procedure[16], a group of intact spheroids was embedded in Spurr's resin. To reveal the structure of spheroids, the resin excess was removed from their surface by

washing with absolute ethanol for 3 seconds before the polymerization in oven at 70°C (**Figure 2E,F**).

In this way, the resin penetrates the intracellular domain and allows for stabilization of the ultrastructures. In fact, the 3D architecture of the spheroids is preserved and the cells' cluster is clearly distinguishable. However, the final removal procedure might induce a nanometer thick layer of polymerized resin around the cellular bodies which covers features, i.e. microvilli, which are otherwise not visible in the spheroids prepared by CPD.

To reveal the inner architecture of the mechanically-sectioned spheroids, FIB milling was further performed on the resin-embedded specimens. First, a region of interest (ROI) was located and preserved by a platinum (Pt) layer deposited *via* ion beam. In some cases, depending on the geometry of the spheroid, a thick layer of gold (~ 50 nm) was deposited prior to the SEM observation and was appropriate to limit charging effects and preserve the ROI. This is in fact valid for smaller spheroids whose mechanical-cut subsections would have a final diameter of about 100-200 µm.

For larger subsections, first a thin film of platinum (~0.2 µm) was deposited with an electron current of 26 nA and a voltage of 30 kV covering a nominal rectangular area of 75 µm by 40 µm (see **Experimental Procedure** and **Supplementary Information S3**). Subsequently, an ion-assisted Pt deposition was performed with an current of 9.3 nA and a voltage of 30 kV, in order to achieve a final Pt thickness of ~ 1µm. Moreover, thicker and more irregular spheroid subsections were covered with an additional Pt layer of ~ 0.2 µm.

Then, a first large area tranch out is performed to remove the material in the surrounding of the ROI.

A rectangular area of 75 µm by 40 µm was located, and the milling was performed with a current of 21 nA at 30 kV, fixing a nominal (for silicon) etching depth of 10 µm. Depending on the structural composition of the spheroid subsections, the resulting cross section could be directly visualizated by the backscattered electrons (BSE) detector, while an additional polishing step is carried out to reduce possible curtaining effect or material re-deposition [24]. We found that at least three subsequent polishing steps at decreasing currents and milling areas gave the best results in terms of smoothness and definition of the target cross section. In fact, we carried out serial-sequential milling steps by fixing currents at 0.79 nA, 21 nA, 93 nA, for areas of 75 µm by 30 µm,

75 µm by 20 µm, 75 µm by10 µm, respectively. The overall FIB cross section milling workflow is summarized in **Supplementary Information S3**.

The ROI visualization was finally achieved through the BSE detector and secondary electron modes (SE, see also **Supplementary Information S4**). However, BSE micrographs allow for high resolution (~ 5 nm, different acquisition currents/voltages have been tested as shown in **Supplementary Information S5**) and high contrast, enlightening areas with different material composition, density and conductivity within the spheroid.

Here, by visualizing several cross sections, we can investigate the effect of the mechanical sectioning at different steps of the staining/embedding procedure. In **Figure 3** are reported the internal structure of spheroids after fixation in glutaraldehyde (step 1, **Figure 3A-C**), and in Spurr's resin embedding before (**Figure 3D-F**) and after polymerization (**Figure 3G-I**) which are named here as step 5 and step 6, respectively. SE micrographs in **Figure 3A,D,G** show an overview of a spheroid subsection where an exemplary cutting plane is identified (white arrows). Analogous micrographs have been also reported in **Supplementary Information S6-S7** and a set of sequential cross sections at a 20 nm pitch have been also collected to visualize a volume of interest (**Supplementary Movie 1**).

Furthermore, the BSE micrographs in **Figure 3** (see also **Supplementary Information S7**) revealed defined nuclei (N), large number of mitochondria (M) with appreciable crests, abundant rough endoplasmic reticulum (rER), extracellular matrix (EC) and tight junctions (TJ). No appreciable vacuoles or similar structures, which would indicate the eradication of organelles due to cutting were detectable[25].

Comparing the inner and outer area of spheroids, we found evidence of compression effects due to mechanical stress as effect of the mechanical cutting when spheroids underwent only primary fixation (step 1).

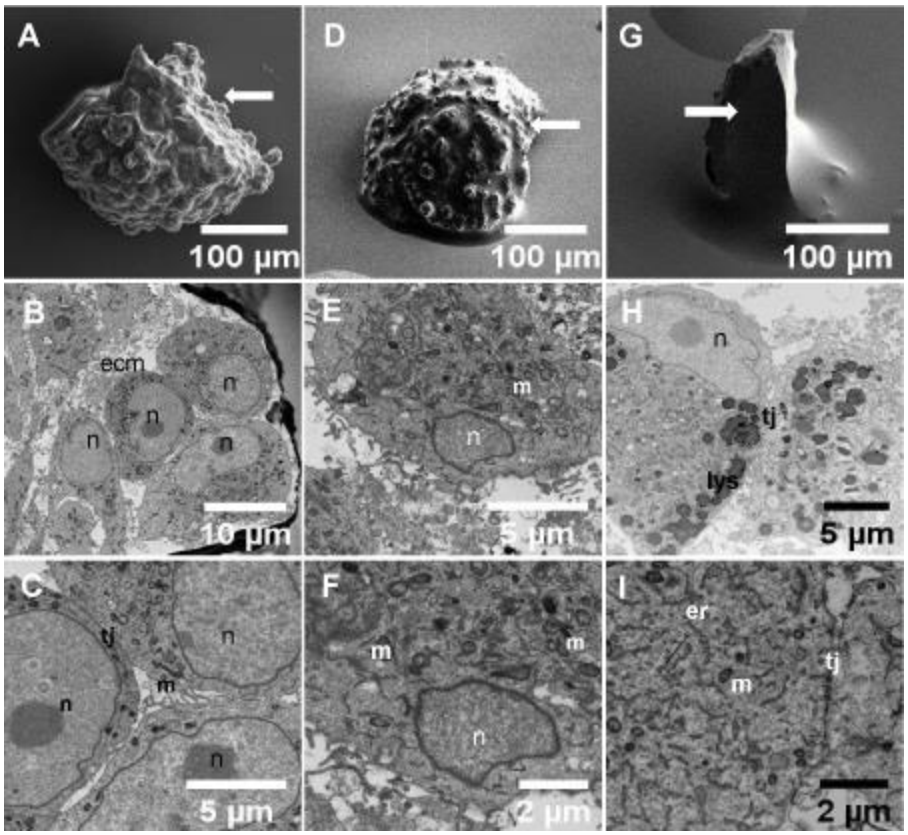

Figure 3: **Characterization of spheroid subsections.** A-C) Scanning electron micrographs (BSE) of U87-MG derived spheroids prepared with ROTO and UTP protocol and resulting cross sections post glutaraldehyde cutting D-F) pre-polymerization cutting, G-I) post-polymerization cutting.

Spheroids subsections obtained after resin embedding prior to polymerization (step 6) were further milled and polished as mentioned earlier.

Finally, we investigated the interface between LMNVs and the outer and inner domains of the tumoral spheroids. The micrographs in **Figure 4E-H** display the different phases occurred during the endocytosis of LMNVs. *Phase I* represents the first contact between the nanovectors and the outer membrane (contact) followed by the formation of membrane invaginations (*phase II*) and then the formation of specific (electron-dense[26]) clathrin-coated pits (*phase III*). **Figure 4H** shows the final LMNVs internalization and their inclusion into vesicles (*phase IV*). In particular, high magnification micrographs revealed the presence of nanovectors in the extracellular matrix domain, in the cytoplasm and incorporated in vacuoles (see **Supplementary Information S8**).

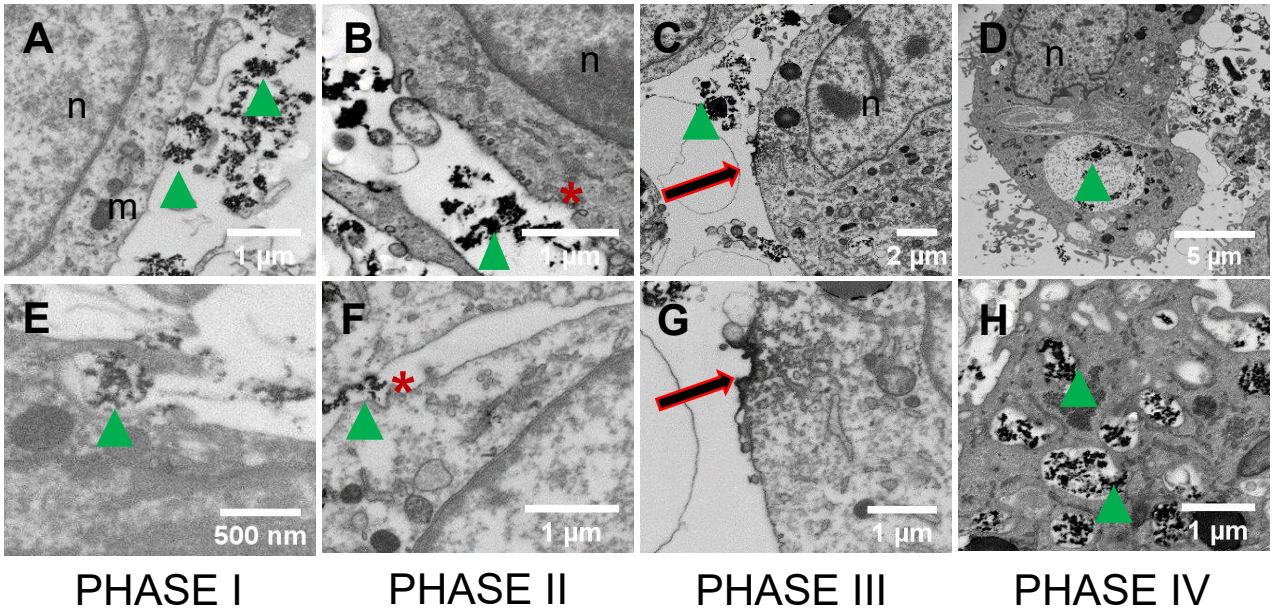

Figure 4: Investigation of nanovectors uptake in spheroids by SEM-FIB.). A-H) SEM micrographs of U87-MG derived spheroids treated with ROTO-UTP protocol after incubation with lipid magnetic nanovectors: backscattered electrons micrographs on inner spheroid cross sections which exhibit diverse nanovectors uptake: phase I- contact; phase II: invagination; phase III: clathrin; phase IV: internalization. N: nuclei, green arrow: LMNVs; black arrow: clathrin; V: vacuoles, red star: invagination.

Conclusions

We showed a procedure for the investigation of 3D tumoral spheroids loaded with lipid magnetic nanovectors. Here, the resolution of the interface allows for the characterization of the cell-nanocarries interaction and the different uptake phases taking place within the spheroid. In order to proceed with localized milling and high resolution imaging, the 3D spheroids have been first mechanically sectioned. The sectioning has been performed at different steps during the heavy-metal staining and the embedding procedure and possible shear stress effects have been evaluated by performing FIB-SEM milling and imaging. Furthermore, we could investigate the cell-cell and cell-extracellular matrix interplay with nanometer resolution and, finally, evaluate the interaction between 3D spheroids and lipid magnetic nanovectors. In conclusion, this study proves a fast artefact-free processing for the nanoscale investigation of 3D complex cellular systems like

spheroids and organoids with nano and macromaterials which more and more are being developed for tissue engineering, bioelectronic and diagnostic platforms.

Experimental Section

Spheroids culture. Cancer spheroids were obtained from glioblastoma multiforme U87-MG cell line (ATCC® HTB-141TM). The composition of the cell medium was Dulbecco Modified Eagle's Medium (DMEM) supplemented with fetal bovine serum (FBS; 10%), L-glutamine (1%), sodium pyruvate (1%), non-essential amino acids (1%), penicillin (100 IU/ml), streptomycin (100 µg/ml). U87 MG cells were cultured in 75 cm^2 flasks with a 20-85 % confluence range. For obtaining the spheroids with the hanging drop method[27], cells were treated with trypsin (0.05% for 5 minutes), centrifuged (300 RCF for 6 minutes) and then resuspended at 10^6 cells/ml concentration. Subsequently, 25 µl drops of cell suspension were deposited upside down on lids of 10 cm diameter Petri dishes and incubated at for 24 hours at 37°C, 5% CO_2 and 100% humidity. The obtained 2D cells aggregates were finally transferred to non-adherent supports consisting in 1% agarose-coated Petri dishes and cultured for 4 days with complete medium for obtaining 3D spheroids.

Fluorescence imaging. For fluorescence labelling and confocal fluorescence microscopy imaging, spheroids were transferred from Petri dishes to 24-well Ibidi®, washed three times with PBS, fixed with 4% paraformaldehyde (PFA) in PBS for 20 minutes at 4°C, labelled with TRITC-phalloidin (100 µM) and Hoechst 33342 (1 µg ml^{-1}). Imaging was carried out with a confocal fluorescence microscopy (C2s system, Nikon) and 3D reconstruction of z-stacks was performed by using NIS Element software (Nikon).

Nanoparticle loading. Lipid magnetic nanovectors (LMNVs) were fabricated as previously described[7], and spheroids were incubated for 24-48 hours with 167 µg/ml of LMNVs.

Fixation and staining for EM. The specimens were prepared following the ultra-thin plasticization (UTP) procedure previously described[17,28]. Spheroids were washed once with 0.1 M sodium cacodylate buffer (EMS, pH 7.2) and then fixed in 2.5% glutaraldehyde solution (Electron Microscopy Sciences, EMS) in the same buffer overnight at 4°C. After washing three times with 0.1 M sodium cacodylate buffer, sample were post fixed in 2% osmium tetroxide/1% potassium ferrocyanide (EMS, RO step), for 1 hour at 4°C in the dark and washed with buffer on ice. Then spheroids were washed with distilled water and kept in water until room temperature was reached. In the meantime, 1% thiocarbohydrazide solution (TCH, EMS) was prepared by

mixing the compound powder and distilled water and heated up at 60°C for 1 hour before filtration. Samples were incubated in TCH solution at room temperature for 20 minutes in the dark (T step) rinsed 3 times with distilled water and post-fixed in 1% osmium tetroxide (O step) for 1 hour at room temperature. After washing with distilled water, they were finally transferred in 0.5% uranyl acetate aqueous solution (EMS) overnight at 4°C in the dark. The next day, spheroids were washed in chilled water and incubated for 3 minutes in 0.15% tannic acid solution (Sigma Aldrich). After washing with water at 4°C, samples were dehydrated in ascending series of ethyl alcohol (Carlo Erba reagents, 30%-50%-70%-95%-100%). Each step was performed for 10 minutes at 4°C. 95% EtOH was performed two times while absolute ethanol step was performed two times at 4°C and for a last time 10 minutes at room temperature. For the sectioning of the spheroids, a razor blade with 30° micro knife (EMS) was used.

***Critical point drying*.** After dehydration, samples were finally prepared for critical point drying (CPD) During the CPD sample preparation, spheroids were placed in a critical point chamber (EM CPD 300, Leica) keeping the level of ethanol to completely immerse the specimens. Then, ethanol was slowly exchanged with liquid CO_2 at 15 °C and 25 cycles of fluid exchange were performed. The heating up process to generate supercritical CO_2 was carried out at 37°C. Starting from 31°C, the supercritical CO_2 turns in to gaseous CO_2. The gas CO_2 is then let out of the chamber through a dedicated valve.

Resin embedding. Spheroids were embedded in epoxy resin (ER) according to the ultra-thin plasticization protocol[16,29] after the dehydration step. The embedding was carried out by exchanging 100% ethanol solution with a mixture of absolute ethanol/Spurr's resin (EMS) with the following ratios and duration: 3:1 for 2 hours; 2:1 for 2 hours; 1:1 overnight; 1:2 for 2 hours; 1:3 for 2 hours. Finally, the mixture was replaced with absolute resin in which spheroids were incubated for one night. Sample were finally embedded in fresh Spurr's two times (3 hours per each step) before polymerization. To avoid damages to the spheroid structure, a glass capillary with a sealed tip was used to collect them from resin and move them to round glass coverslip. Each coverslip was kept in vertical position for 2-3 hours to allow for the excess resin to drain. After the polymerization at 70°C for 24 hours, samples were mounted on a 12 mm aluminum stub using conductive silver paste (RS Company).

SEM/FIB. Samples were covered with a 10-20 nm-thick gold layer *via* sputter coating. Afterwards, they were loaded into a dual beam machine (Helios 650, Thermo Fisher Scientific).

The spheroid surface was scanned with the electron beam at a voltage of 3-5 kV (secondary electrons) to identify a region of interest (ROI).

Once a ROI was located, a first 0.2 µm-thick platinum layer was deposited *via* electron beam-assisted deposition by setting a voltage at 3kV and a current in the range 0.79-9.3 nA. Afterwards, the sample was tilted at 52° to be perpendicular to the ion beam and a second layer of Pt was deposited by ion beam-assisted deposition to reach a final thickness of ~1 µm (in some cases a deposition of an additional 200 nm thick Pt layer was necessary) .

A rectangular-shaped area was located for the milling. Here, the length was always kept at 75 µm while the width varied (depending on the milling step, see **Supplementary Information S4**) in the range 40 – 10 µm and the etching depth was nominally (as for silicon) 10 µm. The ion milling was carried out fixing a voltage at 30 kV and a current in the range of 65 nA-80 pA.

Furthermore, possible curtaining effects and material re-deposition were compensated through milling with lower currents (from 80 pA to 0.23 nA).

Image acquisition was performed in backscattered electrons mode fixing the dwell time at 30 µs, 2 kV as voltage and 0.23 – 0.69 nA as current (dynamic focus built-in function turned on).

References

[1] "Spheroid-based drug screen: considerations and practical approach | Nature Protocols," can be found under https://www.nature.com/articles/nprot.2008.226, **n.d.**

[2] M. Zanoni, F. Piccinini, C. Arienti, A. Zamagni, S. Santi, R. Polico, A. Bevilacqua, A. Tesei, *Scientific Reports* **2016**, *6*, 19103.

[3] "3D tumor spheroids as in vitro models to mimic in vivo human solid tumors resistance to therapeutic drugs - Nunes - 2019 - Biotechnology and Bioengineering - Wiley Online Library," can be found under https://onlinelibrary.wiley.com/doi/10.1002/bit.26845, **n.d.**

[4] E. C. Costa, A. F. Moreira, D. de Melo-Diogo, V. M. Gaspar, M. P. Carvalho, I. J. Correia, *Biotechnol. Adv.* **2016**, *34*, 1427.

[5] A. Marino, A. Camponovo, A. Degl'Innocenti, M. Bartolucci, C. Tapeinos, C. Martinelli, D. D. Pasquale, F. Santoro, V. Mollo, S. Arai, M. Suzuki, Y. Harada, A. Petretto, G. Ciofani, *Nanoscale* **2019**, *11*, 21227.

[6] K. Maier-Hauff, F. Ulrich, D. Nestler, H. Niehoff, P. Wust, B. Thiesen, H. Orawa, V. Budach, A. Jordan, *J Neurooncol* **2011**, *103*, 317.

[7] C. Tapeinos, A. Marino, M. Battaglini, S. Migliorin, R. Brescia, A. Scarpellini, C. D. J. Fernández, M. Prato, F. Drago, G. Ciofani, *Nanoscale* **2018**, *11*, 72.

[8] F. Pampaloni, N. Ansari, E. H. K. Stelzer, *Cell Tissue Res* **2013**, *352*, 161.

[9] K. König, A. Uchugonova, E. Gorjup, *Microscopy Research and Technique* **2011**, *74*, 9.

[10] B. K. Hoffpauir, B. A. Pope, G. A. Spirou, *Nat Protoc* **2007**, *2*, 9.

[11] K. M. Harris, E. Perry, J. Bourne, M. Feinberg, L. Ostroff, J. Hurlburt, *J. Neurosci.* **2006**, *26*, 12101.

[12] J. Jaros, M. Petrov, M. Tesarova, A. Hampl, in *3D Cell Culture: Methods and Protocols* (Ed.: Z. Koledova), Springer New York, New York, NY, **2017**, pp. 417–431.
[13] C. Kizilyaprak, A. G. Bittermann, J. Daraspe, B. M. Humbel, *Methods Mol. Biol.* **2014**, *1117*, 541.
[14] L. H. P. Hekking, M. N. Lebbink, D. a. M. D. Winter, C. T. W. M. Schneijdenberg, C. M. Brand, B. M. Humbel, A. J. Verkleij, J. A. Post, *Journal of Microscopy* **2009**, *235*, 336.
[15] K. Narayan, S. Subramaniam, *Nature Methods* **2015**, *12*, 1021.
[16] X. Li, L. Matino, W. Zhang, L. Klausen, A. F. McGuire, C. Lubrano, W. Zhao, F. Santoro, B. Cui, *Nature Protocols* **2019**, *14*, 1772.
[17] D. Iandolo, F. A. Pennacchio, V. Mollo, D. Rossi, D. Dannhauser, B. Cui, R. M. Owens, F. Santoro, *Advanced Biosystems* **2019**, *3*, 1800103.
[18] A. Friedmann, A. Hoess, A. Cismak, A. Heilmann, *Acta Biomaterialia* **2011**, *7*, 2499.
[19] S. Gopal, C. Chiappini, J. P. K. Armstrong, Q. Chen, A. Serio, C.-C. Hsu, C. Meinert, T. J. Klein, D. W. Hutmacher, S. Rothery, M. M. Stevens, *Advanced Materials* **2019**, *31*, 1900488.
[20] H. E. J. Armer, G. Mariggi, K. M. Y. Png, C. Genoud, A. G. Monteith, A. J. Bushby, H. Gerhardt, L. M. Collinson, *PLoS ONE* **2009**, *4*, e7716.
[21] A. J. Bushby, K. M. Y. P'ng, R. D. Young, C. Pinali, C. Knupp, A. J. Quantock, *Nat. Protocols* **2011**, *6*, 845.
[22] T. Katsumoto, T. Naguro, A. Iino, A. Takagi, *J Electron Microsc (Tokyo)* **1981**, *30*, 177.
[23] M. Lindroth, P. B. Bell, B. A. Fredriksson, *J Microsc* **1988**, *151*, 103.
[24] F. Santoro, E. Neumann, G. Panaitov, A. Offenhäusser, *Microelectronic Engineering* **2014**, *124*, 17.
[25] M. Winey, J. B. Meehl, E. T. O'Toole, T. H. Giddings, *Mol. Biol. Cell* **2014**, *25*, 319.
[26] S. Gopal, C. Chiappini, J. Penders, V. Leonardo, H. Seong, S. Rothery, Y. Korchev, A. Shevchuk, M. M. Stevens, *Adv. Mater. Weinheim* **2019**, *31*, e1806788.
[27] D. Del Duca, T. Werbowetski, R. F. Del Maestro, *J. Neurooncol.* **2004**, *67*, 295.
[28] F. A. Pennacchio, F. Caliendo, G. Iaccarino, A. Langella, V. Siciliano, F. Santoro, *Nano Lett.* **2019**, *19*, 5118.
[29] F. Santoro, W. Zhao, L.-M. Joubert, L. Duan, J. Schnitker, Y. van de Burgt, H.-Y. Lou, B. Liu, A. Salleo, L. Cui, Y. Cui, B. Cui, *ACS Nano* **2017**, *11*, 8320.

Acknowledgements

The authors thank Laura Matino for the help with the UTP procedure and the staff of the Cleanroom Facility at the Central Lab of Istituto Italiano di Tecnologia for the use of the dual-beam microscope.

Probing the ultrastructure of spheroids and their uptake of magnetic nanoparticles by FIB-SEM

Valentina Mollo[1±], Paola Scognamiglio[1±], Attilio Marino[2], Gianni Ciofani[2,3], Francesca Santoro[1*]

[1]Center for Advanced Biomaterials for Healthcare, Istituto Italiano di Tecnologia, Naples, Italy.
[2]Smart Bio-Interfaces, Istituto Italiano di Tecnologia, Pontedera, Italy.
[3]Department of Mechanical and Aerospace Engineering, Politecnico di Torino, Torino, Italy.

SUPPLEMENTARY INFORMATION

Supplementary Movie 1: sequential cross sectioning of a resin embedded spheroid (mechanical cutting performed after resin infiltration) was carried out. 50 frames with a 20 nm pitch were collected. The video is assembled with a speed of 4 frames/sec.

S1 -Technical information concerning cutting steps of spheroids.

Spheroids were divided in to four parts using a razor blade with an orientation of 30°. The procedure was carried out under chemical hood with a stereo-microscope. For the cutting, spheroids were put on a black support on ice to optimize their visualization and keep them refrigerated at the same time. After that, all the ROTO and dehydration steps were carried out in drops laid on Parafilm and the pieces of spheroids were picked up in a minimum volume (2-5 µl). The cutting carried out after the primary fixation (step 1) is challenging because the spheroids are soft and quite transparent. After staining with osmium tetroxide and potassium ferrocyanide both handling and visualization became easier, thanks to the contrast conferred by osmium and at the same time the chemical substance makes the cellular structure more compact and stable, especially the plasma membrane. During the embedding steps, spheroids subsections were placed in a polypropylene vials and collected using a glass capillary with a sealed tip. Before polymerization, each piece was transferred on to a 22x22 mm coverslip and placed in vertical position for 2 hours. After that, the resin excess was washed out with absolute ethanol for 3 seconds, and then dried with filter paper. In some cases, this wash was not necessary (depending on the size of the organoid) due the low viscosity of the resin. In fact, as shown our recent work[17], the choice of resin for the embedding is a crucial point for 3D specimen embedding. All coverslips with spheroids were collected on a silicon mold and put in the oven for the polymerization process at 70°C overnight. In order to evaluate the possible volume change of spheroids during the ROTO-UTP protocol, a group of 12 intact spheroids prepared with the aforementioned protocol. At the each cutting step, brightfield imaging (16X magnification) was performed and the total area of the spheroid was calculated. As shown in the graph, there are no relevant differences in the spheroids' area across all steps of the ROTO protocol.

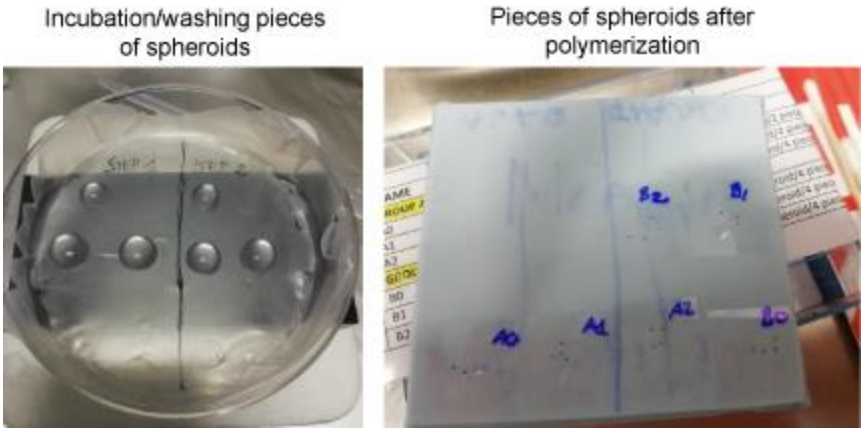

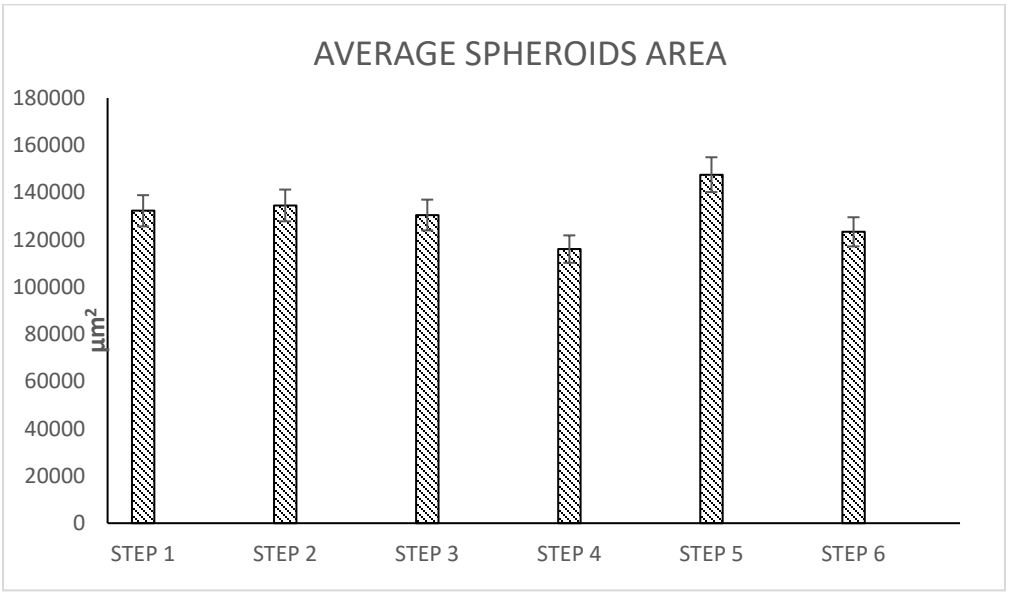

S2-FIB cross sectioning of a spheroid dehydrated *via* CPD.

At an initial observation cells seem to preserve their shapes showing no difference in their external morphology. However, after the FIB milling (**Figure S2-A**) the intracellular domain has a sponge-like structure and no ultrastructures are distinguishable.

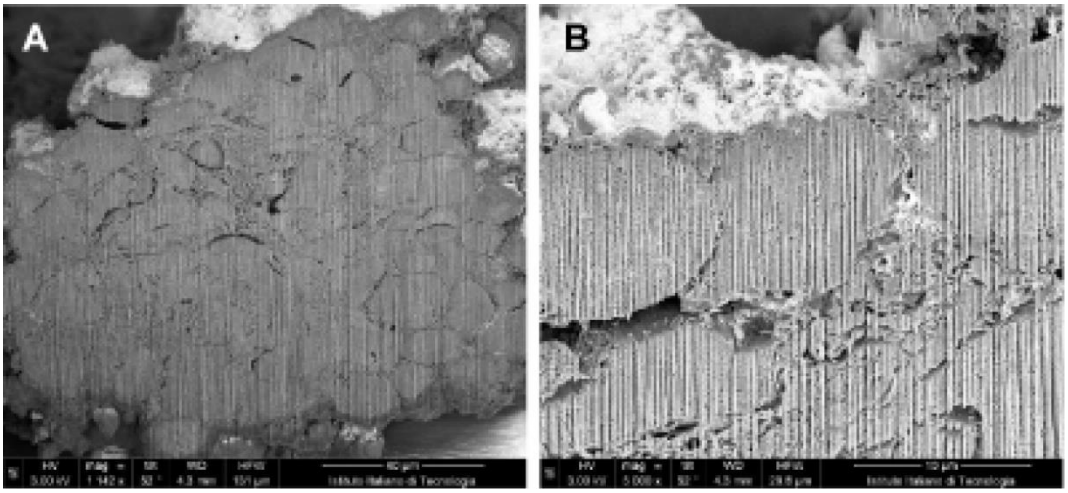

Figure S2 : Scanning electron micrographs of FIB cross sections of CPD specimens.

S3 – FIB cross sectioning procedure.

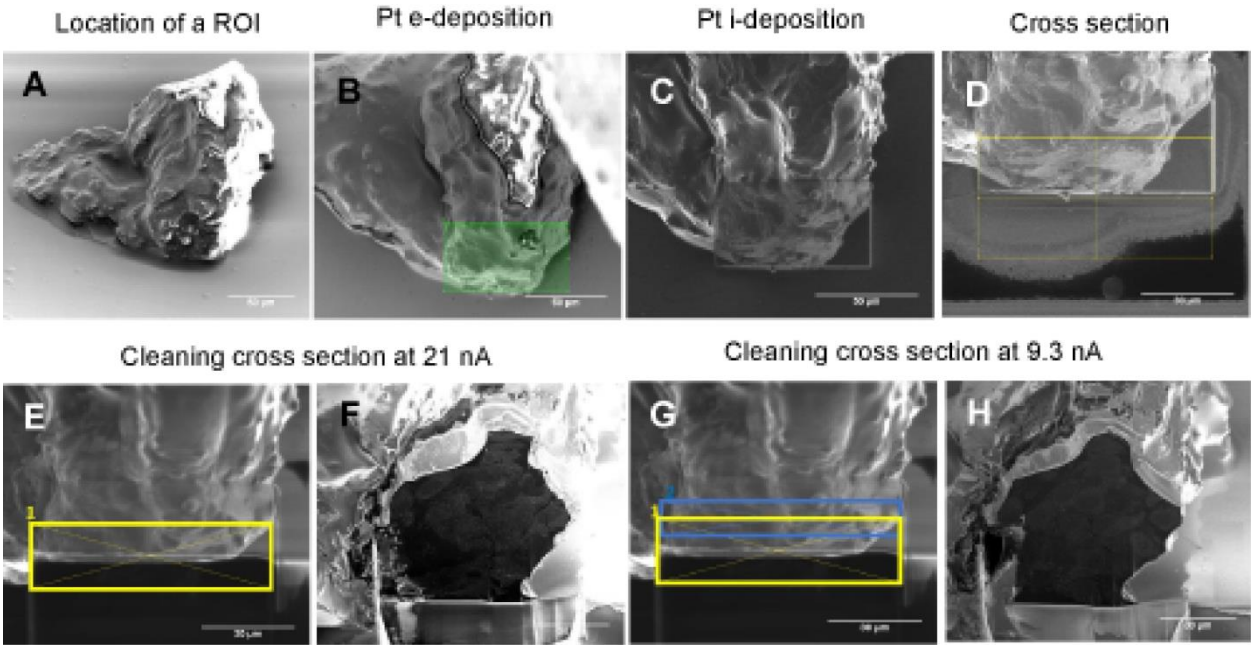

Figure S3: A) location of region of interest (ROI), B) deposition of Pt layer is a rectangular ROI of 75 µm by 40 µm (electron beam assisted) C) Pt ion-beam assisted deposition (area of 75 µm by40 µm), D) ion beam milling, E-F) polishing at 21 nA, G-H) polishing at 9.3 nA.

S4- Imaging by secondary and backscattered electrons detection.

Secondary electrons are very sensitive to the surface of the material and give mainly information its 3D morphology (**Figure S4-C**). Instead, backscattered electrons possess higher energy than secondary electrons thus they are sensitive to the composition of the specimen. Here, the quality of the images depends on the presence of heavy atoms; an area characterized by heavy atoms structures appears bright in the backscattered electron image (**Figure S4-B**) and the shape of borders and internal organelles are clear and well defined (**Figure S4-D**).

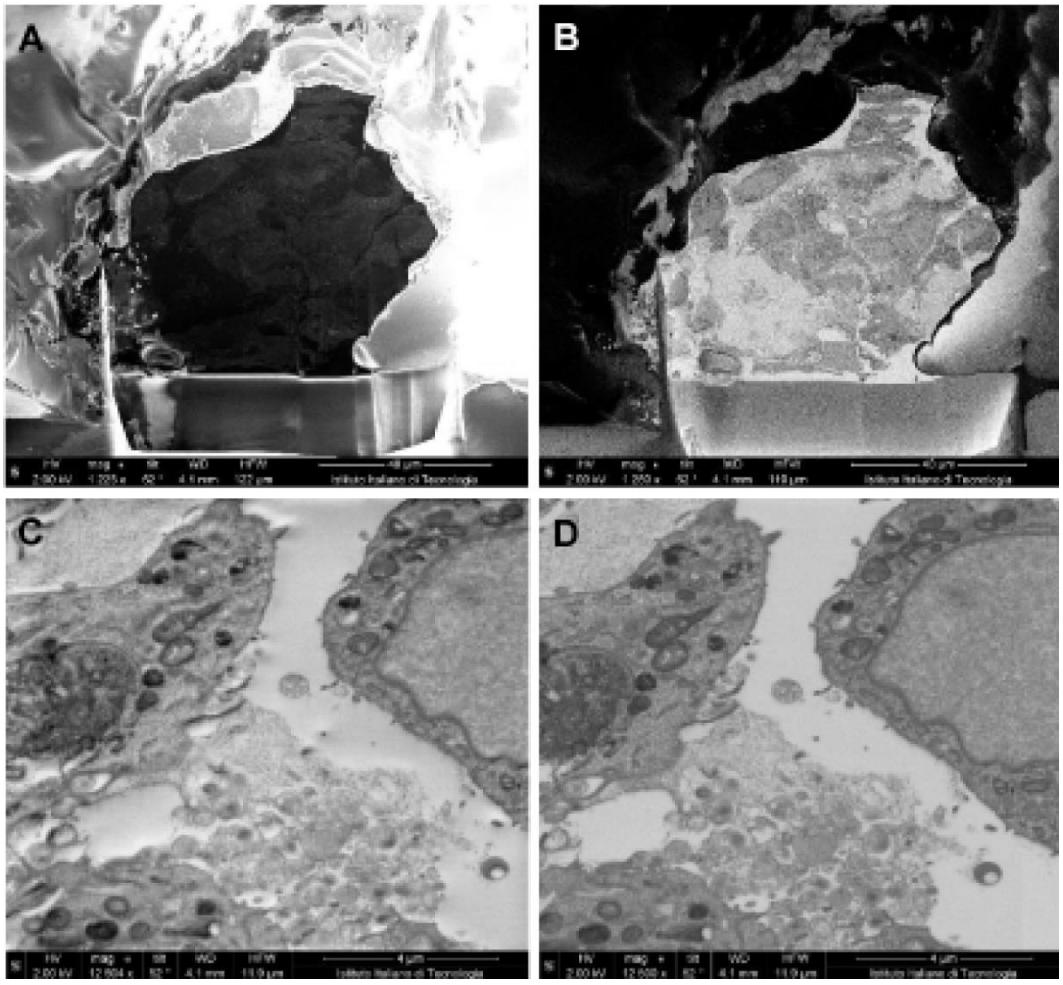

Figure S4 : micrographs acquired with SE A&C) and BSE detectors B&D).

S5 – Image resolution depending on voltage/current in backscattered electrons detection mode.

In **Figure S5,** images of the same area were acquired with the same voltage (2 kV) but increasing current intensity: 0.20 nA, 0.40 nA, 0.80 nA.

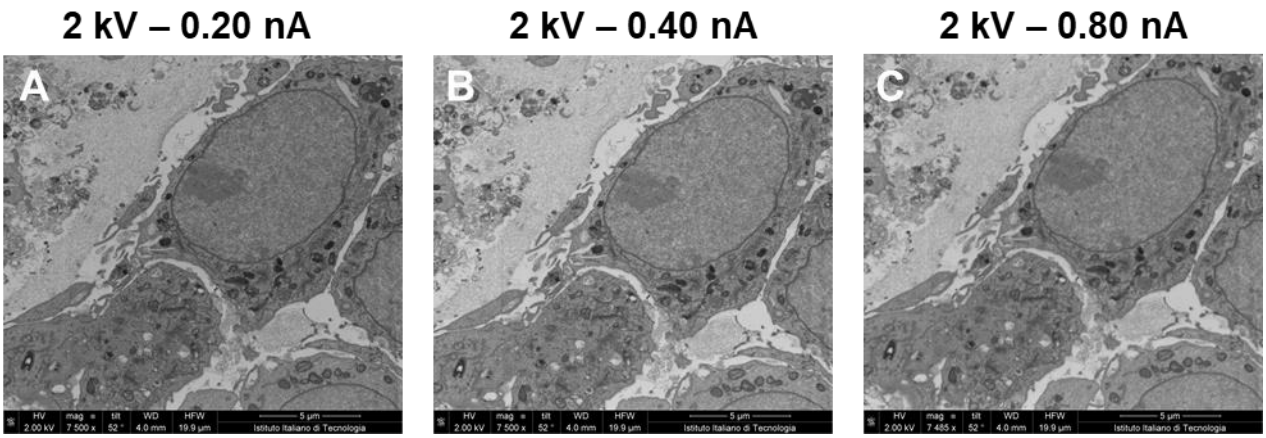

Figure S5: BSE micrographs of the same area acquired at 2 kV and currents of: A) 0.20 nA B) 0.40 nA C) 0.80 nA.

S6- Investigation of ultrastructure in subsection of spheroids obtained by mechanical sectioning after primary fixation in glutaraldehyde (STEP 1).

Figure S6-A depicts the outer part of a spheroid while **Figure S6-B** its inner domain. There are no appreciable damage in organelles or membrane. In fact nuclei, mitochondria, lysosomes, are well preserved, but the cells appear compressed in their outer domains as they underwent mechanical stress during the cut.

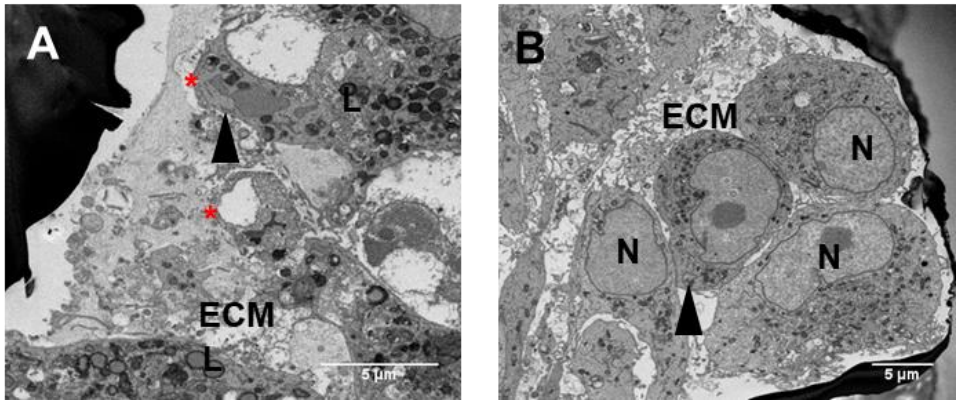

Figure S6: SEM-FIB cross section of U87 derived spheroids after ROTO/UTP protocols at cutting step 1 (after glutaraldehyde fixation) A) external area of spheroids with evidence of cracks (red star), B) inner area of spheroids. N: nuclei, ECM: extracellular matrix, L: lysosomes

S7- Investigation of ultrastructure in subsection of spheroids obtained by mechanical sectioning at STEP 2, STEP 3, STEP 4.

To investigate the possible mechanical damage due the sectioning of spheroids, SEM/FIB cross sections of tree intermediate cutting step are reported after treatment with osmium tetroxide (step 2), after tannic acid (step 3) and before polymerization (Step4). In all micrographs, the cell ultrastructure is well preserved: the cell-cell junctions are evident, and the cytoplasmic organelles are not eradicated or damaged. In fact the cytoplasm is homogenous, the plasma membrane is intact, and some organelles, i.e. mitochondria or nuclei, show their peculiar morphology.

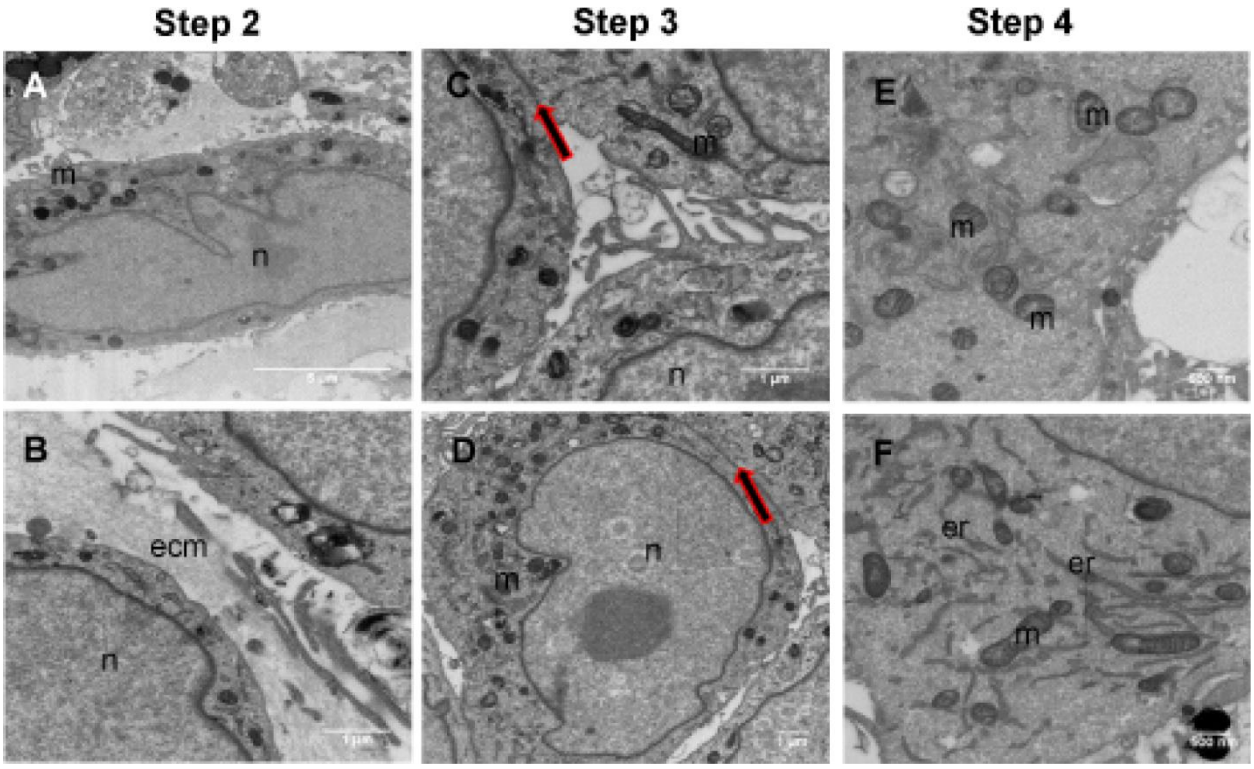

Figure S7:SEM-FIB cross sections of U87 spheroids treated with ROTO protocol: A,B) after osmium tetroxide cutting (step2); C,D) after tannic acid cutting (Step 3); E,F) after Spurr's resin embedding, before polymerization cutting (step 4). Cell-cell junctions are preserved (red/black arrow), mitochondria (m) crests are definite. Also endoplasmic reticulum is well appreciable (er)and extra cellular matrix is compact.

S8- Internalization of nanovectors in to spheroids.

To characterize the internalization of nanovectors at nanometric resolution, spheroids were incubated with LMNVs. SEM/FIB cross section were acquired and the spheroid/nanovector interface was investigated. As shown in **Figure S8,** LMNVs are internalized through endocytosis in vesicles or vacuoles (blu arrows); nanovectors are also found free in cytoplasm (yellow arrow).

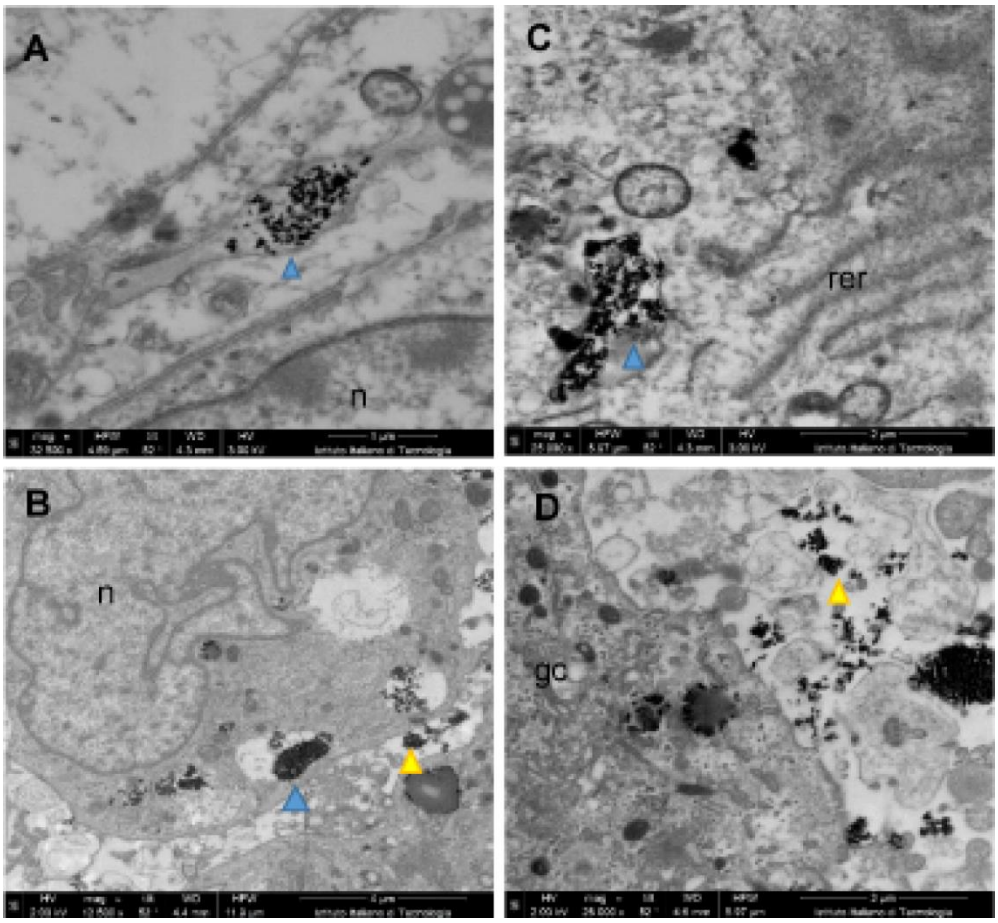

Figure S8: U87 derived spheroids after ROTO and UTO protocol previously incubated with LMNVs. Nanovectors are detected in vacuoles (blu arrow) inside the cell and/or free in cytoplasm (yellow arrows) n: nuclei, gc: Golgi complex, rer: rough endoplasmic reticulum.